ACS APPLIED ENERGY MATERIALS
Cite This: ACS Appl. Energy Mater. XXXX, XXX, XXX−XXX
Letter
www.acsaem.org

Hyperbranched PEO-Based Hyperstar Solid Polymer Electrolytes with Simultaneous Improvement of Ion Transport and Mechanical Strength

Yang Chen,[†,‡,§] Yi Shi,[‡,§] Yanliang Liang,[‡,§] Hui Dong,[‡] Fang Hao,[‡] Audrey Wang,[‡] Yuxiang Zhu,[‡] Xiaoli Cui,[†] and Yan Yao*[,‡]

[†]Department of Materials Science, Fudan University, Shanghai 200433, China

[‡]Department of Electrical and Computer Engineering and Texas Center for Superconductivity, University of Houston, Houston, Texas 77204, United States

Supporting Information

ABSTRACT: Poly(ethylene oxide) (PEO)-based solid polymer electrolytes (SPEs) with nonflammability, shape flexibility, and high SPE/Li interfacial stability are poised to be an enabler for solid-state lithium batteries, but their application is restricted by low room-temperature ionic conductivity and poor mechanical strength at elevated temperatures. Herein, hyperstar polymers are synthesized with hyperbranched PEO serving as the star core and linear polystyrene (PS) serving as the arms. The hyperbranched topological structure suppresses crystallization and facilitates PEO segmental motion, and the steric hindrance for PEO segmental motion is tuned by controlling the average chain length of the branched PEO segments. The rigid PS arms entangle during phase separation and form mechanically strong physical cross-links. An all-solid-state Li/$LiFePO_4$ battery based on our hyperstar SPE delivers a stable capacity of 142 mAh g^{-1} at 0.2C owing to fast ion transport and stable electrolyte/electrode interfaces.

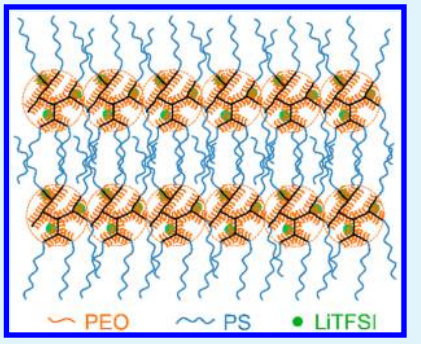

KEYWORDS: *lithium battery, solid polymer electrolyte, poly(ethylene oxide), hyperstar, hyperbranched, polystyrene, cross-linking*

All-solid-state lithium batteries (ASSLBs) have attracted extensive attention as next-generation reliable energy storage devices.[1−4] Solid polymer electrolytes (SPEs) are prospective materials for integration into ASSLBs due to their nonflammability, shape flexibility, mechanical strength, and high electrolyte/electrode interfacial stability.[5−8] These desirable properties of SPEs could potentially solve the issues of flammability and dendritic Li growth that plague the organic liquid electrolytes in commercial lithium ion batteries, and thus, SPEs are able to significantly improve the safety and performance of lithium batteries.[9−11] Poly(ethylene oxide) (PEO)-based SPEs are a promising polymer host for solid electrolytes due to their low glass transition temperature and favorable Li-ion complexation, but their practical applications are restricted by low ionic conductivity at room temperature and poor mechanical strength at elevated temperatures.[12,13] Therefore, it is vital to design and synthesize a PEO-based SPE with a simultaneous improvement of ionic conductivity and mechanical strength.

Li-ion diffusion usually occurs exclusively in the amorphous PEO domains, so a topological structure that is predominantly amorphous benefits Li-ion diffusion. PEO-based SPEs with linear and brushed structures still crystallize considerably at desirable lithium salt concentrations.[14,15] Hyperbranched structures are amorphous and have been recognized as effective for promoting the ionic conductivity of PEO-based SPEs even at room temperature.[16,17] On the other hand, the desirable mechanical strength of PEO-based SPEs is typically achieved by the copolymerization of PEO with rigid chain segments such as polystyrene (PS).[14,15] As demonstrated by the poly(styrene-*block*-ethylene oxide-*block*- styrene) (PS-*b*-PEO-*b*-PS) triblock copolymers (Scheme 1a) and the poly[(norbornene-*graft*-styrene)-*block*-(norbornene-*graft*-ethylene oxide)-*block*-(norbornene-*graft*-styrene)] (*g*PS-*b*-*g*PEO-*b*-*g*PS) brush copolymers (Scheme 1b), the PS fragments entangle to form continuous rigid domains.[14,15] Combining a hyperbranched structure and copolymerization with PS appears to be a rational strategy to simultaneously satisfy the demands of high conductivity and mechanical strength. Li et al. combined a hyperbranched PS (*hb*PS) core and poly[poly(ethylene glycol) methyl ether methacrylate] (PPEGMA) arms to form *hb*PS-*star*-PPEGMA (*hb*PS-*s*-PPEGMA) star polymers in pursuit of a favorable mechanical property,[18] but the *hb*PS behaved as isolated hard spheres with little entanglement (Scheme 1c).[19,20] The mechanical property was improved when linear PS blocks were introduced between the *hb*PS core and the PPEGMA arms to form the *hb*PS-*star*-(PS-*block*-PPEGMA) star polymers,[21] which is probably due to the

Received: December 14, 2018
Accepted: February 25, 2019

DOI: 10.1021/acsaem.8b02188
ACS Appl. Energy Mater. XXXX, XXX, XXX−XXX

Scheme 1. Illustration of the Correlation between Topological Structures and Phase Separation of the PEO-PS Copolymers Blending with LiTFSI: (a) PS-*b*-PEO-*b*-PS Triblock Copolymer,[14] (b) *g*PS-*b*-*g*PEO-*b*-*g*PS Brush Polymer,[15] (c) *hb*PS-*s*-PPEGMA Star Polymer,[18] and (d) *hb*PPEGMA$_m$-*s*-PS$_n$ Hyperstar Polymer

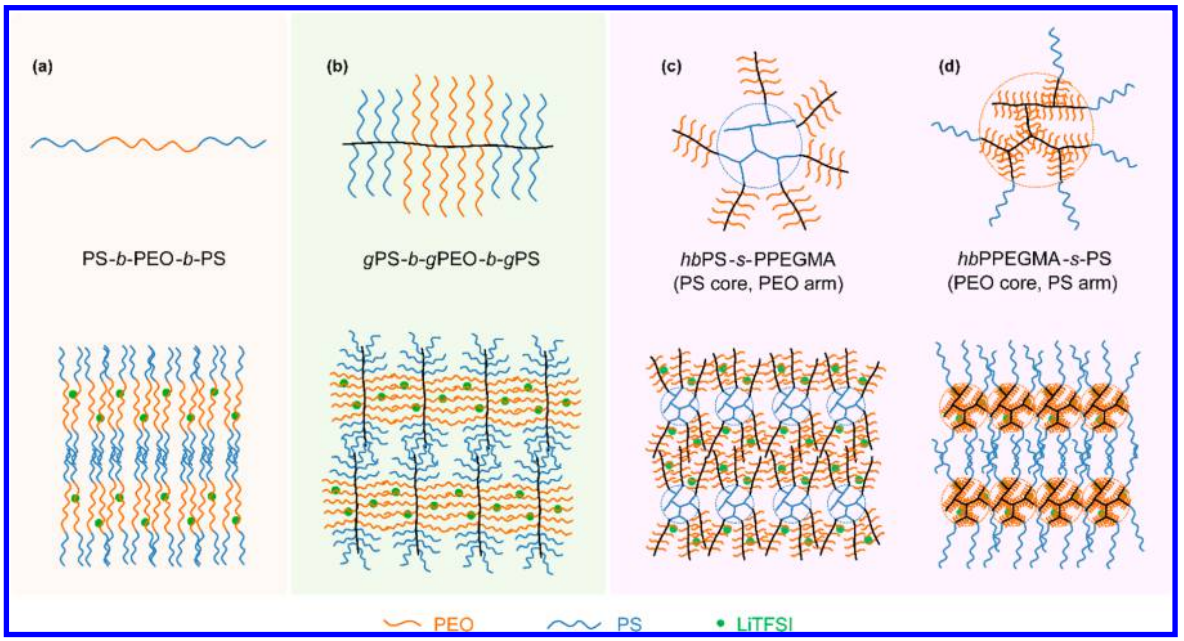

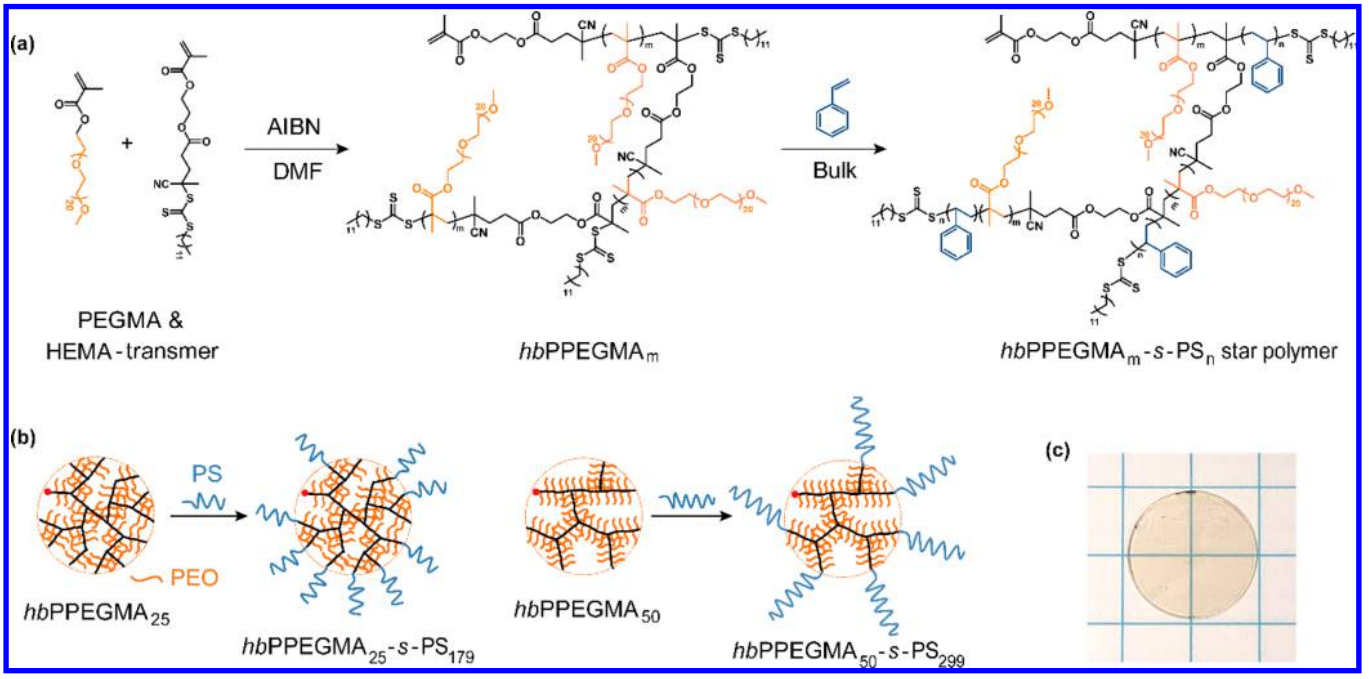

Figure 1. Synthesis of *hb*PPEGMA$_m$-*s*-PS$_n$ hyperstar polymers. (a) Synthetic route. (b) Schematic of hyperbranched *hb*PPEGMA$_m$ and *hb*PPEGMA$_m$-*s*-PS$_n$ polymers with different average chain lengths of branched PEO (m) and linear PS (n). (c) Digital photograph of *hb*PPEGMA$_{50}$-*s*-PS$_{299}$ SPE membrane.

intramolecular entanglement of the linear PS fragments. Still, intermolecular entanglement of PS fragments, which is necessary for forming rigid SPE films, is not realized in these polymers. Thus, judicious placement of PS and PEO fragments in a hyperstar polymer design is crucial for realizing the intended conductivity and mechanical properties.

Herein, we report on hyperbranched PEO-based hyperstar polymers, namely, *hb*PPEGMA$_m$-*s*-PS$_n$ (where m and n stand for the average chain length of branched PEO segments and PS arms, respectively). The hyperbranched PPEGMA core ensures little crystallinity and thus efficient ionic conduction, while the PS arms physically cross-link to provide mechanical strength (Scheme 1d). The SPE based on *hb*PPEGMA$_{50}$-*s*-PS$_{299}$ showed a desirable ionic conductivity of 9.5×10^{-5} S cm^{-1} and a storage modulus of 0.5 MPa at 60 °C. An all-solid-state Li/LiFePO$_4$ battery using this SPE delivered an initial capacity of 132 mAh g^{-1} and maintained 142 mAh g^{-1} after 100 cycles at 0.2C at 60 °C. This stable and high capacity is attributed to the improved Li-ion transport and stable electrolyte/electrode interfaces.

DOI: 10.1021/acsaem.8b02188
ACS Appl. Energy Mater. XXXX, XXX, XXX−XXX

Table 1. Characteristics of the *hb*PPEGMA$_m$-*s*-PS$_n$ Polymers and SPEs

sample[a]	M_n (g mol^{-1})	M_w/M_n	f_{PEO}[b]	E' (MPa)[c]	σ (S cm^{-1})[d]	t_{Li}^+[e]
*hb*PPEGMA$_{25}$-*s*-PS$_{179}$	97.5k	1.25	56	1.4	5.1×10^{-5}	0.13
*hb*PPEGMA$_{50}$-*s*-PS$_{299}$	110.6k	1.35	60	0.5	9.5×10^{-5}	0.22

[a]M_n, M_w/M_n, and f_{PEO} were taken from pristine *hb*PPEGMA$_m$-*s*-PS$_n$ polymers, while E', σ, and t_{Li}^+ were taken from *hb*PPEGMA$_m$-*s*-PS$_n$ SPEs. [b]PEO weight percentage. [c]Storage modulus at 60 °C. [d]Ionic conductivity at 60 °C. [e]Li$^+$ transference number at 60 °C.

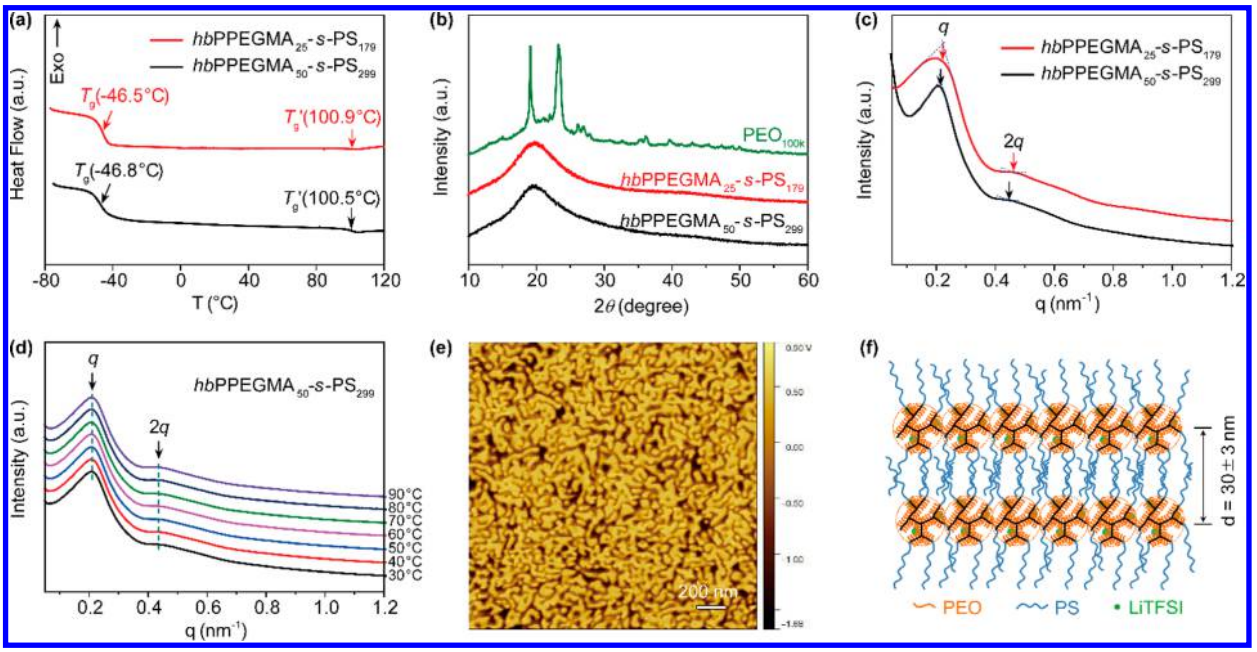

Figure 2. Characterizations of *hb*PPEGMA$_m$-*s*-PS$_n$ SPEs. (a) DSC curves. (b) XRD patterns with PEO$_{100k}$ (M_n = 100 kg mol^{-1}) SPE ([EO]/[Li$^+$] = 16) as a comparison. (c) SAXS diffractograms at room temperature, (d) temperature-dependent SAXS diffractograms, and (e) tapping-mode AFM phase image of *hb*PPEGMA$_{50}$-*s*-PS$_{299}$ SPE. Scale bar: 200 nm. (f) Schematic lamellar structure.

A polymerizable chain transfer agent (CTA) was synthesized from the reaction between 2-hydroxyethyl methacrylate (HEMA) and 4-cyano-4-[(dodecylsulfanylthiocarbonyl)-sulfanyl]pentanoic acid (see the Supporting Information). The presence of the alkenyl functional group in the HEMA-transmer was confirmed by ^{1}H NMR spectrum (Figure S1). As illustrated in Figure 1a, the *hb*PPEGMA$_m$-*s*-PS$_n$ hyperstar polymers were synthesized by a two-step reversible addition–fragmentation chain transfer (RAFT) polymerization.[22] The hyperbranched *hb*PPEGMA$_m$ was synthesized at a feed molar ratio of [poly(ethylene glycol) methyl ether methacrylate (PEGMA)]:[HEMA-transmer] = m:1 with azobis-(isobutyronitrile) (AIBN) as the initiator. The PS chain segments were then introduced via RAFT polymerization of styrene (St) using *hb*PPEGMA$_m$ as macro-CTA at a feed molar ratio of [St]:[macro-CTA] = 1000:1 to obtain *hb*PPEGMA$_m$-*s*-PS$_n$ hyperstar polymers. The molecular weight (M_n) and polydispersity index (M_w/M_n) were characterized by multi-detector gel permeation chromatography (GPC) (Figure S2a, Table 1). The value of m approximately equals the feed molar ratio of [PEGMA]/[HEMA-transmer] since the polymerization conversion rate of *hb*PPEGMA$_m$ is above 98% as confirmed by ^{1}H NMR. The value of n is determined from the integral area ratio of the characteristic peaks of C_6H_5 in PS and OCH_3 in PPEGMA in the ^{1}H NMR spectrum. For *hb*PPEGMA$_{50}$-*s*-PS$_{299}$, the feed molar ratio of [PEGMA]:[HEMA-transmer] is 50:1, and thus m = 50. The integral area ratio of the C_6H_5 and OCH_3 peaks in the ^{1}H NMR spectrum of *hb*PPEGMA$_{50}$-*s*-PS$_n$ (Figure S2b) is calculated to be 9.97, i.e., $(5n)/(3m)$ = 9.97, and thus n = 299. The GPC trace of the hyperbranched *hb*PPEGMA$_{50}$ displayed a monomodal peak (Figure S2a), indicating a low dispersity in molecular weight.[23] The peak shifted toward higher molecular weight in *hb*PPEGMA$_{50}$-*s*-PS$_{299}$. In addition, compared with the ^{1}H NMR spectrum of *hb*PPEGMA$_{50}$, new peaks at 6.22–7.23 ppm emerged for *hb*PPEGMA$_{50}$-*s*-PS$_{299}$ (Figure S2b). These new peaks were attributed to the protons of the benzyl groups in PS, which further confirmed the successful introduction of PS fragments into the hyperstar polymer. Two hyperstar polymers (*hb*PPEGMA$_{25}$-*s*-PS$_{179}$ and *hb*PPEGMA$_{50}$-*s*-PS$_{299}$) were synthesized with roughly the same PEO content (56% and 60% in weight, respectively) but with different average chain lengths of branched PEO segments (m = 25 and 50, respectively) (Figure 1b). The *hb*PPEGMA$_m$-*s*-PS$_n$ SPE membranes were prepared using *hb*PPEGMA$_m$-*s*-PS$_n$ polymers blended with LiTFSI ([EO]/[Li$^+$] = 16) in acetonitrile (ACN) solvent. The [EO]/[Li$^+$] ratio of 16 was a frequently used concentration which has a relatively high ionic conductivity.[24,25] For convenience, "*hb*PPEGMA$_m$-*s*-PS$_n$ SPE" in this work stands for *hb*PPEGMA$_m$-*s*-PS$_n$/LiTFSI solid polymer electrolytes, while "*hb*PPEGMA$_m$-*s*-PS$_n$" represents pristine *hb*PPEGMA$_m$-*s*-PS$_n$ polymers without Li salts. Figure 1c displays the transparent, freestanding *hb*PPEGMA$_{50}$-*s*-PS$_{299}$ SPE membrane, whose average surface roughness (R_a) was measured to be 1.91 nm using AFM topography (Figure S3).

The phase behaviors were studied by differential scanning calorimetry (DSC) and X-ray diffraction (XRD). The DSC curves for both SPEs exhibited a distinct glass transition

DOI: 10.1021/acsaem.8b02188
ACS Appl. Energy Mater. XXXX, XXX, XXX–XXX

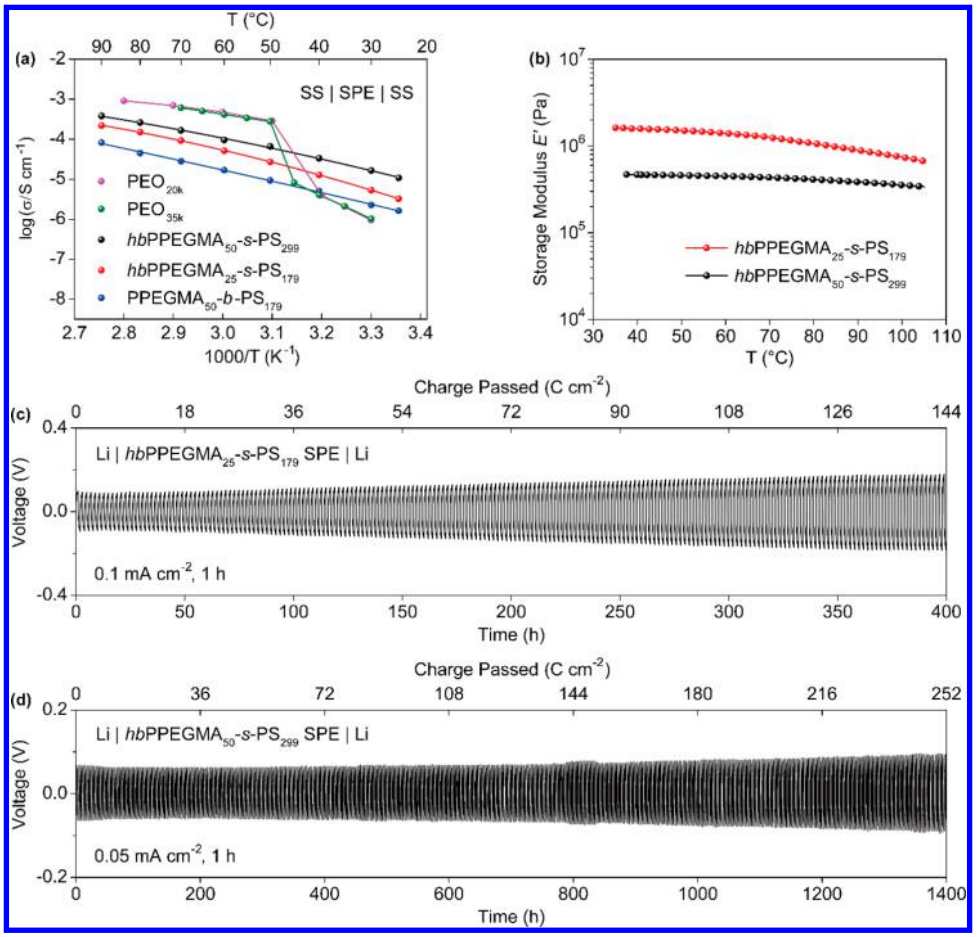

Figure 3. Ionic conductivity and mechanical properties of *hb*PPEGMA$_m$-*s*-PS$_n$ SPEs. (a) Temperature-dependent ionic conductivity. Results from the PEO$_{20k}$ (M_n = 20 kg mol^{-1}) SPEs ([EO]/[Li$^+$] = 20),[31] the PEO$_{35k}$ (M_n = 35 kg mol^{-1}) SPEs ([EO]/[Li$^+$] = 20),[32] and the *hb*PPEGMA$_{50}$-*b*-PS$_{179}$ SPE ([EO]/[Li$^+$] = 16) were shown for comparison. (b) Storage modulus E'. Li plating/stripping voltage profiles versus cycle time and charge passed of Li|*hb*PPEGMA$_m$-*s*-PS$_n$ SPE|Li symmetric cells cycled at 60 °C with 1 h charge and 1 h discharge at a current density of (c) 0.1 mA cm^{-2} for *hb*PPEGMA$_{25}$-*s*-PS$_{179}$ SPE and (d) 0.05 mA cm^{-2} for *hb*PPEGMA$_{50}$-*s*-PS$_{299}$ SPE.

temperature (T_g) for PEO at approximately −47 °C and a weak T_g' for PS at ∼101 °C; additionally, no melting transition was detected (Figure 2a). These results indicate that the *hb*PPEGMA$_m$-*s*-PS$_n$ SPEs were microphase-separated and that PEO crystallization was suppressed thoroughly. The XRD pattern of PEO$_{100k}$ (M_n = 100 kg mol^{-1}) SPE containing only linear PEO chains showed two major characteristic peaks at 2θ = 19.1° and 23.3°, corresponding to the (120) and (112) lattice planes of crystalline PEO, respectively.[19,26] These peaks were absent in the patterns of the *hb*PPEGMA$_m$-*s*-PS$_n$ SPEs (Figure 2b), reflecting their amorphous nature.[11,26] Morphology investigation of the microphase-separated *hb*PPEGMA$_m$-*s*-PS$_n$ SPEs by small-angle X-ray scattering (SAXS) revealed self-assembly into a lamellar structure, as indicated by the primary peak (q) and the higher order peak (2q) with a scattering vector ratio of 1:2 (Figure 2c).[27] The *d*-spacings of *hb*PPEGMA$_{50}$-*s*-PS$_{299}$ and *hb*PPEGMA$_{25}$-*s*-PS$_{179}$ SPE were calculated corresponding to the primary peak at q = ∼0.21 nm^{-1} to be 29.4 and 28.6 nm, respectively.[28] The *d*-spacing is mainly determined by the molecular weight of the entangled segments at a fixed mass or volume ratio of each component.[27,29] The molecular weight of the PS segments in *hb*PPEGMA$_{50}$-*s*-PS$_{299}$ and *hb*PPEGMA$_{25}$-*s*-PS$_{179}$ is 44.2 and 42.9 kg mol^{-1}, respectively, with the former being 3% higher. Thus, it is reasonable that these two *hb*PPEGMA$_m$-*s*-PS$_n$ SPEs have similar *d*-spacings. The structural stability of the assembly was demonstrated by the unchanged SAXS diffractograms from 30 to 90 °C (Figure 2d). The tapping-mode AFM phase image of *hb*PPEGMA$_{50}$-*s*-PS$_{299}$ SPE shows clear fingerprint-like patterns (Figure 2e), reflecting the vertical orientation of the lamellar structure.[20,30] The *d*-spacing was measured to be 30 ± 3 nm in the phase image, which agreed with the SAXS result. As illustrated in Figure 2f, PS arms rearrange and entangle after phase separation.[20] The lamellar structure is then formed by alternating self-assembled PS and PEO layers.

The ionic conductivities of PEO-based SPEs including *hb*PPEGMA$_m$-*s*-PS$_n$ and PPEGMA$_{50}$-*b*-PS$_{179}$, which is a linear polymer we synthesized with a similar PPEGMA−PS ratio (see Supporting Information for synthesis details), were determined by SS|SPE|SS (SS = stainless steel) symmetric cells (Figure 3a). The conductivities of SPEs containing linear homopolymers PEO$_{20k}$ and PEO$_{35k}$ are also included for comparison.[31,32] A turning point emerged at around 40−50 °C for both PEO$_{20k}$ and PEO$_{35k}$ SPEs, reflecting a phase transition process due to the crystalline phase melting. In contrast, the ionic conductivity of the *hb*PPEGMA$_m$-*s*-PS$_n$ SPEs increased quasilinearly with no turning points, indicating little crystallinity of the PEO domains. The room-temperature ionic conductivities of *hb*PPEGMA$_m$-*s*-PS$_n$ SPEs were 5−16 times higher than those of PEO$_{20k}$ and PEO$_{35k}$ SPEs and 2−7 times

DOI: 10.1021/acsaem.8b02188
ACS Appl. Energy Mater. XXXX, XXX, XXX−XXX

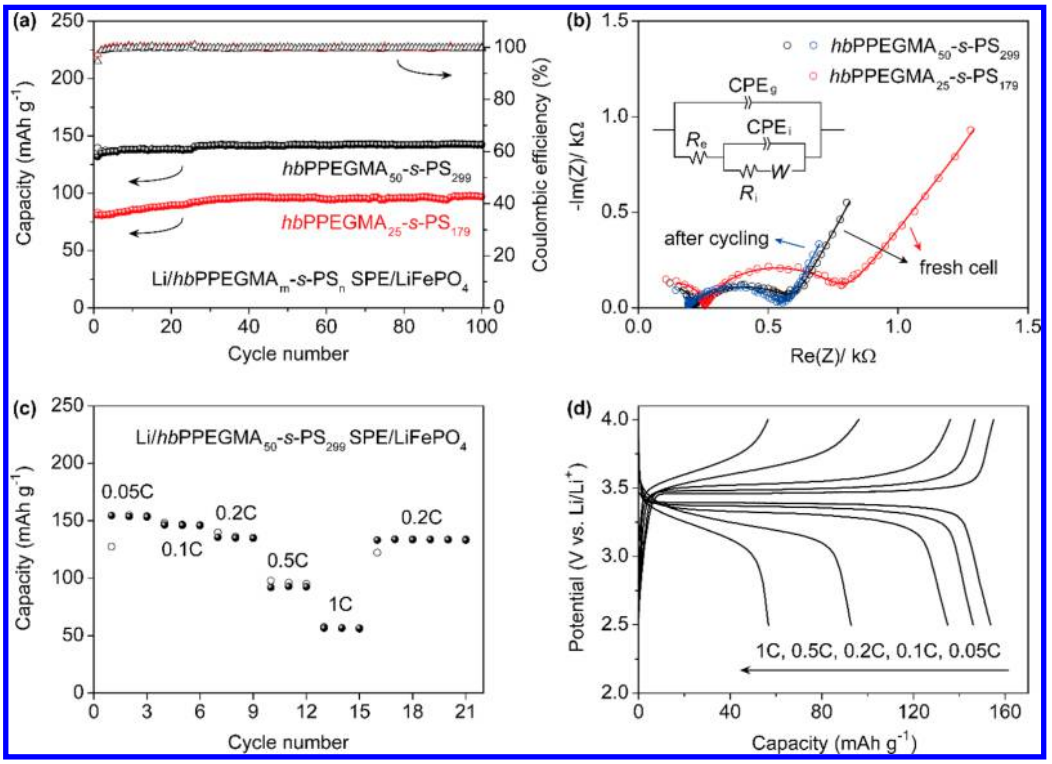

Figure 4. Electrochemical properties of Li/*hb*PPEGMA$_m$-*s*-PS$_n$ SPE/LiFePO$_4$ cells at 60 °C. (a) Cycling performance at 0.2C. (b) Nyquist plots before and after 100 charge/discharge cycles (inset shows the equivalent circuit[43]). (c) Specific capacities and (d) voltage profiles at different current rates using *hb*PPEGMA$_{50}$-*s*-PS$_{299}$ SPE.

that of the linear PPEGMA$_{50}$-*b*-PS$_{179}$ SPE. The ionic conductivity of *hb*PPEGMA$_{50}$-*s*-PS$_{299}$ SPE (9.5×10^{-5} S cm^{-1}) was twice that of *hb*PPEGMA$_{25}$-*s*-PS$_{179}$ SPE (5.1×10^{-5} S cm^{-1}) at 60 °C. The enhancement of ionic conduction was attributed to the doubled average chain length of branched PEO segments, which provided abundant local structural relaxation.[16,17,33] Because the ionic conduction of *hb*PPEGMA$_m$-*s*-PS$_n$ SPEs involves the segmental motion of PEO chains, the Vogel−Tammann−Fulcher (VTF) equation (Figure S4),[34,35] rather than a simple Arrhenius model,[36] was selected to fit ionic conductivities. The ionic transport activation energies (E_a) of *hb*PPEGMA$_{50}$-*s*-PS$_{299}$ and *hb*PPEGMA$_{25}$-*s*-PS$_{179}$ SPEs are fitted to be 10.0 and 10.2 kJ mol^{-1}, respectively (Table S1). The Li$^+$ transference number (t_{Li}^+) was determined by the Bruce−Vincent method through a chronoamperometry technique coupled with AC impedance using Li|SPE|Li symmetric cells (Figure S5).[37] The t_{Li}^+ of *hb*PPEGMA$_{50}$-*s*-PS$_{299}$ SPE ($t_{Li}^+ = 0.22$) was 1.7 times that of *hb*PPEGMA$_{25}$-*s*-PS$_{179}$ SPEs ($t_{Li}^+ = 0.13$) (Table S2), resulting in an even higher Li-ion conductivity for the former.[25,38] We note that the Li$^+$ transference number obtained using the Bruce−Vincent method, based on the assumption of diluted solutions, is an approximate value. The true transference number of polymer electrolytes can be measured rigorously using Newman's method.[39]

The mechanical properties of the *hb*PPEGMA$_m$-*s*-PS$_n$ SPEs were measured by dynamic mechanical analysis (DMA) under a tensile mode. Figure 3b shows that *hb*PPEGMA$_{25}$-*s*-PS$_{179}$ SPE has the higher storage modulus of 1.4 MPa at 60 °C, while the strength of *hb*PPEGMA$_{50}$-*s*-PS$_{299}$ SPE was more consistent over the temperature range of battery operation. To investigate the Li/SPE interfacial property, the impedance of the Li|*hb*PPEGMA$_{25}$-*s*-PS$_{179}$ SPE|Li symmetric cell was monitored at 60 °C. Both the bulk and interfacial resistances remain nearly constant during 210 h of rest (Figure S6), indicating a high Li−SPE chemical compatibility. The Li|*hb*PPEGMA$_m$-*s*-PS$_n$ SPE|Li cell was cycled at 1 h charging and 1 h discharging at 60 °C to measure the Li stripping/plating behavior. The Li|*hb*PPEGMA$_{25}$-*s*-PS$_{179}$ SPE|Li cell cycled for 400 h at 0.1 mA cm^{-2} without Li dendrite failure. The cross-sectional SEM images clearly show that the Li plating is homogeneous, and no dendrites are observed at the Li/SPE interface (Figure S7). The charge passed is 144 C cm^{-2} (Figure 3c) with an average voltage increase of 0.6 mV C^{-1} cm^2 (Figure S8a). The voltage increase mainly originates from the increased Li-SPE interfacial resistance (Figure S9); this phenomenon of voltage increase was also reported in Li's work.[40] The average voltage increase is only 0.1 mV C^{-1} cm^2 for the Li|*hb*PPEGMA$_{50}$-*s*-PS$_{299}$ SPE|Li cell (Figure S8b). The charge passed for the Li|*hb*PPEGMA$_{50}$-*s*-PS$_{299}$ SPE|Li cell is 252 C cm^{-2} (Figure 3d), which is comparable to the value reported by Stone et al.[41] These results indicate that the Li/SPE interface is stable and that the mechanical strength of the SPEs is capable of suppressing Li dendrite growth.

The above characterizations led to a deeper understanding of the topological structure design for physically cross-linked polymer electrolytes. With both being star-shaped, our *hb*PPEGMA-*s*-PS SPE and the *hb*PS-*s*-PPEGMA SPE reported by Li et al.[18] show ionic conductivities within a half order of magnitude (~1×10^{-4} S cm^{-1} for the former and 4×10^{-4} S cm^{-1} for the latter at 60 °C) owing to sufficient segmental mobility of PEO chains in both polymers. However, the mechanical properties are largely different. The SPE based on *hb*PS-*s*-PPEGMA is a sticky liquid at 25 °C, which is a result of *hb*PS behaving as a hard, condensed sphere surrounded by PEO chains without further intermolecular entanglement.[19,42]

DOI: 10.1021/acsaem.8b02188
ACS Appl. Energy Mater. XXXX, XXX, XXX−XXX

In contrast, the linear PS arms of *hb*PPEGMA-*s*-PS entangle intermolecularly to form mechanically strong physical cross-links. A solid-state SPE membrane can be easily processed and applied in lithium batteries meeting the simultaneous demands of fast ionic transport and blocking Li dendrite growth.

The linear sweep voltammetry curve of the Li|*hb*PPEG-MA_{50}-*s*-PS_{299} SPE|SS cell reveals electrolyte anodic stability of up to 4.34 V (Figure S10). This potential is determined using an empirical rule when the anodic current density reaches 0.012 mA cm^{-2}.[44,45] The suitability of the SPEs for ASSLBs was evaluated by testing Li-$LiFePO_4$ (LFP) cells at 60 °C. After 100 charge/discharge cycles at 0.2C (1C = 170 mA g^{-1}), the charge passed for Li/SPE/LFP cells was 150 and 100 C cm^{-2} using *hb*PPEGMA$_{50}$-*s*-PS$_{299}$ and *hb*PPEGMA$_{25}$-*s*-PS$_{179}$ SPEs, respectively (Figure S11). The charge passed was lower than the value reported by Hallinan et al.[46] due to a lower mass loading of $LiFePO_4$ active materials (1.5 mg cm^{-2} in this work). With the *hb*PPEGMA$_{50}$-*s*-PS$_{299}$ SPE, the initial discharge capacity was 132 mAh g^{-1}, and a stable capacity of 142 mAh g^{-1} was maintained after 100 cycles (Figure 4a). This stable capacity based on the physically cross-linked *hb*PPEG-MA_{50}-*s*-PS_{299} SPE was higher than that of PEO-based hybrid SPEs and was comparable to that of chemically cross-linked SPEs (Figure S12). The interfacial resistance (R_i in the equivalent circuit model) equals the diameter of the semicircle in the high−medium frequency region of the Nyquist plot in Figure 4b.[43] The initial interfacial resistances of *hb*PPEGMA$_{50}$-*s*-PS$_{299}$ and *hb*PPEGMA$_{25}$-*s*-PS$_{179}$ SPEs were fitted to be 394.5 and 533.7 Ω, respectively (Table S3). Thus, the faster Li-ion conduction of the *hb*PPEGMA$_{50}$-*s*-PS$_{299}$ SPE and more rapid interfacial charge transfer resulted in a higher reversible capacity, which was 1.5 times that of the cell with a *hb*PPEGMA$_{25}$-*s*-PS$_{179}$ SPE. The cycling stability was attributed to a stable electrolyte/electrode interface, since the interfacial resistance after 100 cycles (342.9 Ω) is slightly lower than that of a fresh cell (394.5 Ω) (Figure 4b and Table S3). The interfacial impedance variation per cycle is −0.1%, exhibiting a stable interface compared with those from the literature (Table S4). The Li/*hb*PPEGMA$_{50}$-*s*-PS$_{299}$ SPE/LFP cell delivered a capacity of 154, 146, 135, 93, and 57 mAh g^{-1} at 0.05C, 0.1C, 0.2C, 0.5C, and 1C, respectively (Figure 4c), and the capacity recovered when the current was reverted to 0.2C. The corresponding voltage profiles are shown in Figure 4d. The clean plateaus demonstrate an absence of side reactions at the tested current densities.

In conclusion, hyperstar polymers *hb*PPEGMA$_m$-*s*-PS$_n$ were synthesized via a two-step RAFT polymerization. Improved Li^+ transport (~0.1 mS cm^{-1} at 60 °C) was demonstrated by the synthesized hyperstar polymers due to the suppressed crystallization of the PEO domains. The mechanical property was simultaneously enhanced by the efficient entanglement of linear PS arms after phase separation. The all-solid-state Li/*hb*PPEGMA$_{50}$-*s*-PS$_{299}$ SPE/LFP cell maintained 142 mAh g^{-1} after 100 cycles at 0.2C at 60 °C. Therefore, this work provides a new strategy for designing solid polymer electrolytes to meet the simultaneous demands of ionic conduction, mechanical strengthening, and stable electrolyte/electrode interfaces for integration into all-solid-state lithium batteries.

■ ASSOCIATED CONTENT

Supporting Information

The Supporting Information is available free of charge on the ACS Publications website at DOI: 10.1021/acsaem.8b02188.

Materials and experimental procedures, NMR spectra and GPC traces, AFM topographic images, VTF fitting of ionic conductivity, SEM images of cross-section of Li|SPE|Li cell after cycling, LSV curves of Li|SPE|SS cell, and comparison of electrochemical performance of PEO-based SPEs (PDF)

■ AUTHOR INFORMATION

Corresponding Author

*E-mail: yyao4@uh.edu.

ORCID

Yang Chen: 0000-0003-0108-8342
Yi Shi: 0000-0003-2943-5465
Yanliang Liang: 0000-0001-6771-5172
Hui Dong: 0000-0003-0169-0069
Fang Hao: 0000-0002-7701-6874
Audrey Wang: 0000-0002-8642-4546
Yuxiang Zhu: 0000-0001-5688-5600
Xiaoli Cui: 0000-0001-9958-4517
Yan Yao: 0000-0002-8785-5030

Author Contributions

§Y.C., Y.S., and Y.L. contributed equally to this work.

Notes

The authors declare no competing financial interest.

■ ACKNOWLEDGMENTS

Y.Y. acknowledges funding support from the U.S. Department of Energy's Office of Energy Efficiency and Renewable Energy (EERE), as part of the Battery 500 Consortium (award DE-EE0008234). Y.C. acknowledges the funding from the China Scholarship Council (No. 201706100064). We thank Dr. Xiaobing Zuo for valuable discussion of SAXS data. Use of the facilities at Sector 12-ID-B at APS was supported by the U.S. Department of Energy, Office of Science, Office of Basic Energy Science, under Contract DE-AC02-06CH11357. We thank Prof. Haleh Ardebili and Dr. Mengying Yuan for the use of dynamic mechanical analysis equipment.

■ REFERENCES

(1) Tarascon, J. M.; Armand, M. Issues and Challenges Facing Rechargeable Lithium Batteries. *Nature* **2001**, *414*, 359−367.
(2) Manthiram, A.; Yu, X.; Wang, S. Lithium Battery Chemistries Enabled by Solid-State Electrolytes. *Nat. Rev. Mater.* **2017**, *2*, 16103.
(3) Liu, K.; Liu, Y.; Lin, D.; Pei, A.; Cui, Y. Materials for Lithium-Ion Battery Safety. *Sci. Adv.* **2018**, *4*, No. eaas9820.
(4) Hao, F.; Han, F.; Liang, Y.; Wang, C.; Yao, Y. Architectural Design and Fabrication Approaches for Solid-State Batteries. *MRS Bull.* **2018**, *43*, 775−781.
(5) Morris, M. A.; An, H.; Lutkenhaus, J. L.; Epps, T. H. Harnessing the Power of Plastics: Nanostructured Polymer Systems in Lithium-Ion Batteries. *ACS Energy Lett.* **2017**, *2*, 1919−1936.
(6) Zhai, H.; Xu, P.; Ning, M.; Cheng, Q.; Mandal, J.; Yang, Y. A Flexible Solid Composite Electrolyte with Vertically Aligned and Connected Ion-Conducting Nanoparticles for Lithium Batteries. *Nano Lett.* **2017**, *17*, 3182−3187.
(7) Fan, L.; Wei, S.; Li, S.; Li, Q.; Lu, Y. Recent Progress of the Solid-State Electrolytes for High-Energy Metal-Based Batteries. *Adv. Energy Mater.* **2018**, *8*, 1702657.
(8) Mackanic, D. G.; Michaels, W.; Lee, M.; Feng, D.; Lopez, J.; Qin, J.; Cui, Y.; Bao, Z. Crosslinked Poly(tetrahydrofuran) as a Loosely Coordinating Polymer Electrolyte. *Adv. Energy Mater.* **2018**, *8*, 1800703.

DOI: 10.1021/acsaem.8b02188
ACS Appl. Energy Mater. XXXX, XXX, XXX−XXX

(9) Duan, H.; Yin, Y. X.; Shi, Y.; Wang, P. F.; Zhang, X. D.; Yang, C. P.; Shi, J. L.; Wen, R.; Guo, Y. G.; Wan, L. J. Dendrite-Free Li-Metal Battery Enabled by a Thin Asymmetric Solid Electrolyte with Engineered Layers. *J. Am. Chem. Soc.* **2018**, *140*, 82−85.
(10) Fan, W.; Li, N. W.; Zhang, X.; Zhao, S.; Cao, R.; Yin, Y.; Xing, Y.; Wang, J.; Guo, Y. G.; Li, C. A Dual-Salt Gel Polymer Electrolyte with 3D Cross-Linked Polymer Network for Dendrite-Free Lithium Metal Batteries. *Adv. Sci.* **2018**, *5*, 1800559.
(11) Cui, Y.; Liang, X.; Chai, J.; Cui, Z.; Wang, Q.; He, W.; Liu, X.; Liu, Z.; Cui, G.; Feng, J. High Performance Solid Polymer Electrolytes for Rechargeable Batteries: A Self-Catalyzed Strategy toward Facile Synthesis. *Adv. Sci.* **2017**, *4*, 1700174.
(12) Xue, Z.; He, D.; Xie, X. Poly(ethylene oxide)-Based Electrolytes for Lithium-Ion Batteries. *J. Mater. Chem. A* **2015**, *3*, 19218−19253.
(13) Mindemark, J.; Lacey, M. J.; Bowden, T.; Brandell, D. Beyond PEO−Alternative Host Materials for Li^+-Conducting Solid Polymer Electrolytes. *Prog. Polym. Sci.* **2018**, *81*, 114−143.
(14) Beaudoin, E.; Phan, T. N.; Robinet, M.; Denoyel, R.; Davidson, P.; Bertin, D.; Bouchet, R. Effect of Interfaces on the Melting of PEO Confined in Triblock PS-*b*-PEO-*b*-PS Copolymers. *Langmuir* **2013**, *29*, 10874−10880.
(15) Bates, C. M.; Chang, A. B.; Momčilović, N.; Jones, S. C.; Grubbs, R. H. ABA Triblock Brush Polymers: Synthesis, Self-Assembly, Conductivity, and Rheological Properties. *Macromolecules* **2015**, *48*, 4967−4973.
(16) Lee, S.-I.; Schömer, M.; Peng, H.; Page, K. A.; Wilms, D.; Frey, H.; Soles, C. L.; Yoon, D. Y. Correlations between Ion Conductivity and Polymer Dynamics in Hyperbranched Poly(ethylene oxide) Electrolytes for Lithium-Ion Batteries. *Chem. Mater.* **2011**, *23*, 2685−2688.
(17) Itoh, T.; Horii, S.; Uno, T.; Kubo, M.; Yamamoto, O. Influence of Hyperbranched Polymer Structure on Ionic Conductivity in Composite Polymer Electrolytes of PEO/Hyperbranched Polymer/$BaTiO_3$/Li Salt System. *Electrochim. Acta* **2004**, *50*, 271−274.
(18) Ren, S.; Zheng, T.; Zhou, Q.; Zhang, L.; Li, H. Preparation and Ionic Conductivity of Composite Polymer Electrolytes Based on Hyperbranched Star Polymer. *Ionics* **2014**, *20*, 1225−1234.
(19) Niitani, T.; Amaike, M.; Nakano, H.; Dokko, K.; Kanamura, K. Star-Shaped Polymer Electrolyte with Microphase Separation Structure for All-Solid-State Lithium Batteries. *J. Electrochem. Soc.* **2009**, *156*, A577−A583.
(20) Jang, S.; Lee, K.; Moon, H. C.; Kwak, J.; Park, J.; Jeon, G.; Lee, W. B.; Kim, J. K. Vertical Orientation of Nanodomains on Versatile Substrates through Self-Neutralization Induced by Star-Shaped Block Copolymers. *Adv. Funct. Mater.* **2015**, *25*, 5414−5419.
(21) Ren, S.; Chang, H.; He, L.; Dang, X.; Fang, Y.; Zhang, L.; Li, H.; Hu, Y.; Lin, Y. Preparation and Ionic Conductive Properties of All-Solid Polymer Electrolytes Based on Multiarm Star Block Polymers. *J. Appl. Polym. Sci.* **2013**, *129*, 1131−1142.
(22) Semsarilar, M.; Perrier, S. 'Green' Reversible Addition-Fragmentation Chain-Transfer (RAFT) Polymerization. *Nat. Chem.* **2010**, *2*, 811−820.
(23) Shi, Y.; Cao, X.; Hu, D.; Gao, H. Highly Branched Polymers with Layered Structures that Mimic Light-Harvesting Processes. *Angew. Chem., Int. Ed.* **2018**, *57*, 516−520.
(24) Marzantowicz, M.; Krok, F.; Dygas, J. R.; Florjańczyk, Z.; Zygadło-Monikowska, E. The Influence of Phase Segregation on Properties of Semicrystalline PEO: LiTFSI Electrolytes. *Solid State Ionics* **2008**, *179*, 1670−1678.
(25) Pożyczka, K.; Marzantowicz, M.; Dygas, J. R.; Krok, F. Ionic Conductivity and Lithium Transference Number of Poly(ethylene oxide): LiTFSI System. *Electrochim. Acta* **2017**, *227*, 127−135.
(26) Barthel, M. J.; Rudolph, T.; Teichler, A.; Paulus, R. M.; Vitz, J.; Hoeppener, S.; Hager, M. D.; Schacher, F. H.; Schubert, U. S. Self-Healing Materials via Reversible Crosslinking of Poly(ethylene oxide)-*block*-poly(furfuryl glycidyl ether) (PEO-*b*-PFGE) Block Copolymer Films. *Adv. Funct. Mater.* **2013**, *23*, 4921−4932.
(27) Singh, M.; Odusanya, O.; Wilmes, G. M.; Eitouni, H. B.; Gomez, E. D.; Patel, A. J.; Chen, V. L.; Park, M. J.; Fragouli, P.; Iatrou, H.; Hadjichristidis, N.; Cookson, D.; Balsara, N. P. Effect of Molecular Weight on the Mechanical and Electrical Properties of Block Copolymer Electrolytes. *Macromolecules* **2007**, *40*, 4578−4585.
(28) Panday, A.; Mullin, S.; Gomez, E. D.; Wanakule, N.; Chen, V. L.; Hexemer, A.; Pople, J.; Balsara, N. P. Effect of Molecular Weight and Salt Concentration on Conductivity of Block Copolymer Electrolytes. *Macromolecules* **2009**, *42*, 4632−4637.
(29) Chang, A. B.; Bates, C. M.; Lee, B.; Garland, C. M.; Jones, S. C.; Spencer, R. K. W.; Matsen, M. W.; Grubbs, R. H. Manipulating the ABCs of Self-Assembly via Low-χ Block Polymer Design. *Proc. Natl. Acad. Sci. U. S. A.* **2017**, *114*, 6462−6467.
(30) Chaudhury, S.; Gaalken, J.; Meyer, J.; Ulbricht, M. Calorimetric Studies of PEO-*b*-PMMA and PEO-*b*-PiPMA Diblock Copolymers Synthesized via Atom Transfer Radical Polymerization. *Polymer* **2018**, *139*, 11−19.
(31) Kim, B.; Chae, C.-G.; Satoh, Y.; Isono, T.; Ahn, M.-K.; Min, C.-M.; Hong, J.-H.; Ramirez, C. F.; Satoh, T.; Lee, J.-S. Synthesis of Hard−Soft−Hard Triblock Copolymers, Poly(2-naphthyl glycidyl ether)-*block*-poly[2-(2-(2-methoxyethoxy)ethoxy)ethyl glycidyl ether]-*block*-poly(2-naphthyl glycidyl ether), for Solid Electrolytes. *Macromolecules* **2018**, *51*, 2293−2301.
(32) Bouchet, R.; Phan, T. N. T.; Beaudoin, E.; Devaux, D.; Davidson, P.; Bertin, D.; Denoyel, R. Charge Transport in Nanostructured PS−PEO−PS Triblock Copolymer Electrolytes. *Macromolecules* **2014**, *47*, 2659−2665.
(33) Jo, G.; Kim, O.; Kim, H.; Hyeok Choi, U.; Lee, S.-B.; Jeong Park, M. End-Functionalized Block Copolymer Electrolytes: Effect of Segregation Strength on Ion Transport Efficiency. *Polym. J.* **2016**, *48*, 465−472.
(34) Prasanth, R.; Shubha, N.; Hng, H. H.; Srinivasan, M. Effect of Poly(ethylene oxide) on Ionic Conductivity and Electrochemical Properties of Poly(vinylidenefluoride) Based Polymer Gel Electrolytes Prepared by Electrospinning for Lithium Ion Batteries. *J. Power Sources* **2014**, *245*, 283−291.
(35) Diederichsen, K. M.; Buss, H. G.; McCloskey, B. D. The Compensation Effect in the Vogel−Tammann−Fulcher (VTF) Equation for Polymer-Based Electrolytes. *Macromolecules* **2017**, *50*, 3831−3840.
(36) Chi, X.; Liang, Y.; Hao, F.; Zhang, Y.; Whiteley, J.; Dong, H.; Hu, P.; Lee, S.; Yao, Y. Tailored Organic Electrode Material Compatible with Sulfide Electrolyte for Stable All-Solid-State Sodium Batteries. *Angew. Chem., Int. Ed.* **2018**, *57*, 2630−2634.
(37) Evans, J.; Vincent, C. A.; Bruce, P. G. Electrochemical Measurement of Transference Numbers in Polymer Electrolytes. *Polymer* **1987**, *28*, 2324−2328.
(38) Diederichsen, K. M.; McShane, E. J.; McCloskey, B. D. Promising Routes to a High Li^+ Transference Number Electrolyte for Lithium Ion Batteries. *ACS Energy Lett.* **2017**, *2*, 2563−2575.
(39) Pesko, D. M.; Timachova, K.; Bhattacharya, R.; Smith, M. C.; Villaluenga, I.; Newman, J.; Balsara, N. P. Negative Transference Numbers in Poly(ethylene oxide)-Based Electrolytes. *J. Electrochem. Soc.* **2017**, *164*, E3569−E3575.
(40) Pan, Q.; Smith, D. M.; Qi, H.; Wang, S.; Li, C. Y. Hybrid Electrolytes with Controlled Network Structures for Lithium Metal Batteries. *Adv. Mater.* **2015**, *27*, 5995−6001.
(41) Stone, G. M.; Mullin, S. A.; Teran, A. A.; Hallinan, D. T.; Minor, A. M.; Hexemer, A.; Balsara, N. P. Resolution of the Modulus versus Adhesion Dilemma in Solid Polymer Electrolytes for Rechargeable Lithium Metal Batteries. *J. Electrochem. Soc.* **2012**, *159*, A222−A227.
(42) Ishizu, K.; Kojima, T.; Ohta, Y.; Shibuya, T. Nanopattern Formation on Polymer Substrate Using Star-Hyperbranched Nano-spheres. *J. Colloid Interface Sci.* **2004**, *272*, 76−81.
(43) Liu, Y.; Gorgutsa, S.; Santato, C.; Skorobogatiy, M. Flexible, Solid Electrolyte-Based Lithium Battery Composed of $LiFePO_4$ Cathode and $Li_4Ti_5O_{12}$ Anode for Applications in Smart Textiles. *J. Electrochem. Soc.* **2012**, *159*, A349−A356.

DOI: 10.1021/acsaem.8b02188
ACS Appl. Energy Mater. XXXX, XXX, XXX−XXX

(44) Wang, X.; Yasukawa, E.; Mori, S. Inhibition of Anodic Corrosion of Aluminum Cathode Current Collector on Recharging in Lithium Imide Electrolytes. *Electrochim. Acta* **2000**, *45*, 2677−2684.
(45) Hallinan, D. T.; Rausch, A.; McGill, B. An Electrochemical Approach to Measuring Oxidative Stability of Solid Polymer Electrolytes for Lithium Batteries. *Chem. Eng. Sci.* **2016**, *154*, 34−41.
(46) Hallinan, D. T.; Mullin, S. A.; Stone, G. M.; Balsara, N. P. Lithium Metal Stability in Batteries with Block Copolymer Electrolytes. *J. Electrochem. Soc.* **2013**, *160*, A464−A470.

DOI: 10.1021/acsaem.8b02188
ACS Appl. Energy Mater. XXXX, XXX, XXX−XXX